Innovative Miniature Emittance Scanner Integrating Heat Exchanger in Harsh Vacuum Environment

Vitaly Haslavsky[1], Aviel Edelstein[1], David Dadoun[1], Ido Silverman[2]
[1]Azrieli College of Engineering
26 Yaakov Shreibom Street, Jerusalem, Israel
vitaliha@jce.ac.il
[2]Soreq Nuclear Research Center (SNRC)
Yavne, Israel
ido.silverman@gmail.com

Abstract - This article details different aspects of developing a miniature Allison emittance scanner device. The device demonstrates an original design, incorporating small dimensions that integrate the cooling mechanism within the device itself: $50 \times 30 \times 30$ (Length [mm]$\times$width [mm]$\times$height [mm]). The geometry that was designed for the device includes a unique array of fins and channels directing the flow of the coolant in the most effective configuration. The research and development of the device was executed in collaboration with the Soreq Applied Research Accelerator Facility (SARAF) at the Soreq Nuclear Research Center (SNRC). The final product has a satisfactory mechanical and thermal design of the emittance scanner-heat-exchanger mechanism, and will be implemented by the facility. Special emphasis was given to the choice of materials since the device will be implemented in a high-vacuum environment requiring high levels of purity; the device interacts with an ion beam which may cause radioactive activation in certain metals. Additionally, the device can withstand heat flux of up to 40 MW/m^2 validated through numerical calculations. The ion beam is composed of Deuteron ions carrying 40 keV. The device supplies ample solution to all criteria ensuring adequate function of the device within the beam path of the particle accelerator at SARAF.

Keywords: Emittance scanner, Ion beam accelerator, Cooling mechanism.

1. Introduction

SARAF maintains an ion beam accelerator for the purposes of research, study and medical applications. To name a few, it serves the following purposes: radiation therapy, the science of material research, and nuclear physics research. For example, to treat cancer using radiology, doctors use the fact that cancerous tumors prioritize energy intake when the body is low on fuel. A patient awaiting radiology treatment is required to fast beforehand and the SARAF produces radioactive solutions mixed with sugar that are then given to the patient. The tumor is radiated from the inside, killing or severely damaging it. The significance of the accelerator is great since these radioactive elements have a very short life span, meaning they cannot be imported before the treatment, and they must be injected into the patient within a few hours of production. Another major use for the particle accelerator is the research of materials in the field of material science.

Safe operation of the device requires minimizing particle loss along the accelerator and beaming line in order to diminish activation and radiation hazards. Such losses occur due to fabrication inaccuracies, misalignment of components and repulsion between the positively charged particles in the beam which act upon each other to generate dispersion in the beam along its path. This can be partially compensated by fine-tuning the magnetic and electric fields in the lenses installed along the accelerator, which require accurate measurement of the beam emittance. The beam dispersion is a function of the radial velocity distribution of the particles and a function of the particle position across the beam path. Figure 1 presents typical emittance measurements in X&X' directions, respectively, where Z is the beam direction, and X&X' are the two components of the particle radial velocity. Feschenko [1] achieved very similar results.

There are various methods to measure beam emittance, but most of them require a large space along the beam line 0[2]. One critical point in the SARAF accelerator where such a measurement is required is located between the LEBT (Low Energy Beam Transport and the RFQ (Radio Frequency Quadrupole) where space is limited. Due to the physical restraints

at the desired location, only a space of 50mm in length is available for the task of performing an emittance measurement on the deuteron ion-beam. The only device that can measure in such a limited space is a miniature Allison scanner.
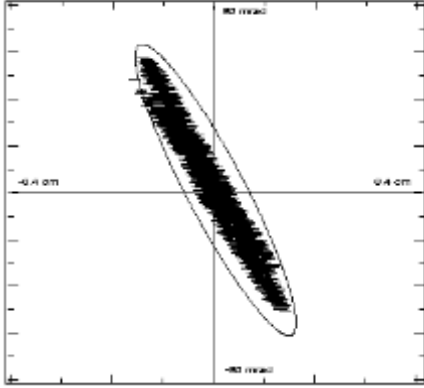

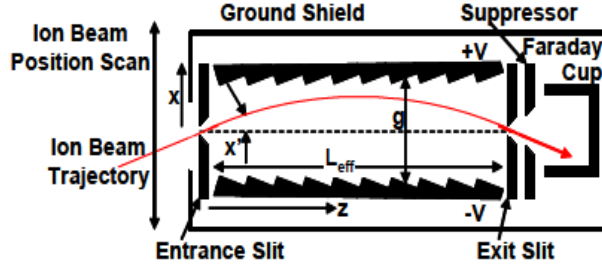Fig. 1: Typical emittance measurement in X-X' direction.

Fig. 2: The cross section of a typical Allison type scanner.

Figure 2 depicts the measuring method of an Allison emittance scanner [3]. From the left, along the Z axis, the beam collides with the device. There is a narrow slit in the center of the device that allows a small fraction of the particle beam to enter the inner cavity. The particles which pass through the slit start to disperse as they continue to travel in the direction of the beam until they reach a second slit. This second slit partially blocks the way into a Faraday cup (FC) which can accurately measure the current collected. Only particles which have zero traverse velocity will pass through the second slit and be measured by the FC. However, ion beam particles are electrically charged and will react to an electric field when acted upon. Therefore, two electrodes placed along the beam path between the two slits are used to deflect the particles. Now, particles with some initial traverse velocity will arrive at the second slit position and be measured by the FC, as illustrated by the red path in Figure 2. As the voltage between the electrodes is increased, particles with higher traverse velocity will be measured by the FC. This process can be repeated along the x-axis to map the whole distribution along the beam. The relationship between the angle of the particle, or the magnitude of the directional component, can be expressed this way [4]:

$$V_{max} = \pm 2 \times \frac{g_e \times x' \times U}{L_{eff}} \tag{1}$$

where: V_{max} is the maximum applicable voltage between the electrodes in volts, g_e is the gap between the two stair-tips of the electrodes in millimeters, x' is the angle a particle has when it crosses the entrance slit in mill radians, U is the energy or the particle in mega electron volts, L_{eff} is the effective length of the electrodes along the device length in millimeters. The requirements of the facility for this device dictate its physical, geometrical, and thermal attributes, such as: the design of a heat exchanger placed in an Allison type scanner; geometrical constraints of 50mm in length, 30mm in width and height; returning water temperature of 50ºC maximum; scanning resolution of ±0.1 mm/step to ensure the position of the scanner is known at all times and is detailed enough for the scan; reducing the overall scan times from up to 60 minutes to 60 seconds. Withstanding beam power of up to 400W emitted on small surface areas.

2. Study method

A system was designed to withstand the worse possible scenario. This was determined by the maximum beam power. It was required that the Allison scanner could diagnose a Deuteron beam of a current of up to 10mAand energy of 40keV which leads to the calculation for maximum beam power:

$$P_{beam} = 10\,[mA] \times 40[KeV] = 400\,[W] \tag{2}$$

As seen in various other design studies [5, 6], due to the physical constraints the scanner plates were divided into three parts: (i) protective plate, (ii) front scanner plate, (iii) back scanner plate or exit plate. The parts (ii) and (iii) are identical regarding the dimension of the slit gap.

The protective plate, as its name suggests, protects the rest of the device from the heat power generated by the ion beam and is allowed to absorb as much heat as possible. As only a small fraction of the beam is diagnosed at any given time, while the rest of the beam creates high-intensity heating on the plate, the heat needs to dissipate. We were able to calculate the power of the beam and derived the percentage of heat that falls into each component of the device (Table 1).

Table 1: the statistical analysis to determine the portions of particles in each section of the beam path.

	σ (SD)	units	2.00	1.00	0.50
1	Max heat on protective plate	[%]	94.09%	92.03%	84.14%
2	Max heat on slit plate	[%]	3.86%	7.65%	14.59%
3	Heat that passes through both slits	[%]	0.07%	1.26%	4.92%
4	Protective slit gap	[mm]	0.2	0.2	0.2
5	Scanner slit gap	[mm]	0.1	0.1	0.1

In Figure 3, σ refers to the Standard Deviation in Gaussian distribution. It indicates what percentage of specimen lies within each range. 64% of the total specimen lies within the 1 σ range from the mean value. Changing the size of σ changes the geometrical circle encasing 64% of the specimen. It should be noted that within the range between negative 4 σ and positive 4 σ lies 100% of the specimen. We refer to the dimensions <x,x'> when dealing with a 2D Gaussian distribution. The "area" encased by the first σ becomes 40.96%. Our intention in calculating the amount of heat that falls on each part of a σ is to get an idea of what to expect for each case. As stated earlier, the 4D Gaussian distribution is an assumption.
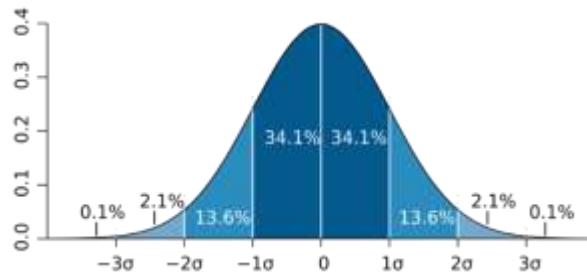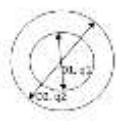

Fig. 3: Standard deviation area.

The main variable that dictates what percentage falls on which component is the slit gap dimension; the smaller the scanner slit gap, the smaller the protective slit gap, allowing it to cover a larger fraction of the ion beam. Another element to consider is the power that falls upon the Faraday Cup, considering its small dimensions and relatively high-power beam. We derived the percentage of the total power that it receives from a statistical calculation which yields an order of magnitude for the amount of particles colliding with each component of the device. It was discovered that when 10W of power fall on the Faraday Cup the Allison scanner can be kept at approximately 400K with water cooling on both sides of the Faraday Cup. The first step towards dealing with this challenge is to model a solid object representing the surfaces of the device and apply the calculated heat power; σ becomes 63.8 % of the beam is applied on a different area accordingly and we use numerical calculations to simulate the problem. The model used is based on molybdenum with a heat conduction coefficient of k=100W/mK. As for the boundary conditions, we use constant temperature for the convection on the opposite face to where the ion beam collides with the device. In the simulation, we set the convection coefficient to h=10kW/m²K; this simulates water dissipating the heat from the focal point. A convection coefficient of this magnitude correlates to the value we expect the water cooling system to have. The convection coefficient of a fluid is not a constant, it differs with the flow

regime and velocities as well as roughness of the wall, for the purpose of the study we estimated an expected average value of the convection coefficient to be 10kW/m²K.

Table 2 details the various configurations considered, where D_1=2.5mm, the case correlates to σ= 1mm, but for D_1=5mm, the case correlates to σ =2mm. Our aspiration is for the scanner to be able withstand a beam that has an σ = 0.5mm but our analysis deals with a less concentrated beam.

Table 2: Circle simplification for the thermal study.

Case	D_1 [mm]	D_2 [mm]	q_1,q_2 [W]	$T_{const\ wall}$ [K]	k [W/mK]	T_{min} [K]	T_{max} [K]
1.1	2.5	8	200	303	100	324.6	1021.17
1.2	2.5	8	200	313	100	334.2	1031.17
1.3	2.5	8	200	323	100	344.2	1041.17
2.1	5	12	200	303	100	332	629.5
2.2	5	12	200	313	100	342	639.5
2.3	5	12	200	323	100	352	649.5

3. Results

Figure 4 simulates the behavior of the protective plate when acted upon by the ion beam. We modeled a circle of various sizes representing the σ value. And as an outcome we can divide the total beam power into geometrical areas. We then set the middle circle to a specific temperature and received the results for the temperature distribution from numerical calculations. The goal of the simulation is to obtain the temperature profile within the solid, radially. The results shows that the center of the circle has a temperature of 1021K for σ=1mm, and 639K for σ=2mm.

Table 3 refers to the second phase of the simulation; the portion of the ions that do not collide with the protective plate collide with the scanner plate after a brief moment. We now seek to analyze what the temperature distribution might look like on the scanner plate. Using this geometry allows us to approximate the temperatures that will fall on the outer side of the scanner plate. The rectangles are derivatives of what is left of the ion beam after it has hit the protective plate. What does not hit a solid material falls on the second plate or goes through it.

Table 3: Rectangular simplification for the scanner plate.

Case	s [mm]	D_1 [mm]	D_2 [mm]	q_1 [Mw/m²]	q_2 [Mw/m²]	$T_{const\ wall}$ [K]	h [kW/m²K]	k [W/mK]	T_{min} [K]	T_{max} [K]
3	0.2	2.5	7.5	40	10	303	10	100	304	402
4	0.5	2.5	7.5	40	10	303	10	100	308	518
5	0.2	5	11.5	10	2.5	303	10	100	303	331
6	0.5	5	11.5	10	2.5	303	10	100	304	364

One of the values received from this study is illustrated in Figure 4: case 4, when the slit gap is 0.5mm shows the temperature distribution throughout the solid. We can see the maximum temperature is 518K in the center.
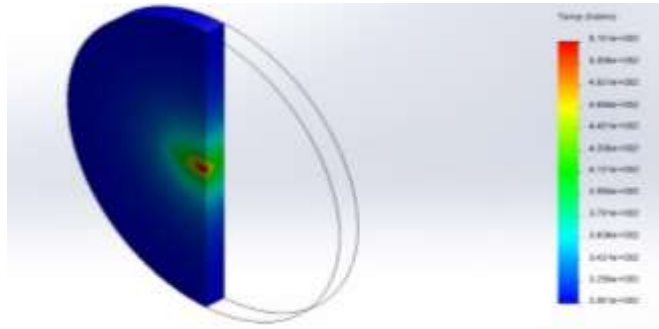
Fig. 4: Cross section of the heat transfer analysis, case 4mm - 0.5mm slit gap.

The Faraday Cup (FC) is located at the end of the device. It is used as a measuring instrument; a wire is attached to an arbitrary point in the Faraday Cup and is connected to a current meter. When an ion collides with the FC it changes the amount of charge in it [7, 8, 9, 10 and 11]. This charge change can be used to measure current on the Faraday Cup which can be calculated as number of particles (i.e. the measurement we need to perform). The circular shape of the Faraday Cup statistically negates the effect of secondary electron emissions, as described in several works [2, 10, 12, 13, 14 and 15]. Schultz and Pomerantz [16] have discussed secondary electron emission as a function of temperature in the solid material which is considerably important for our case. Ziegler and Biersack [17] have derived the thickness of the Faraday Cup material.

In essence, when a charged particle collides with a metallic solid an electron can be deflected from the surface of the metal as a result of the energy involved in the collision.

Regarding the Faraday Cup, we calculate that the power falling in it is 10W and falls onto an squire of 1mm². In the simulation (Figure 5) the results are as follows:
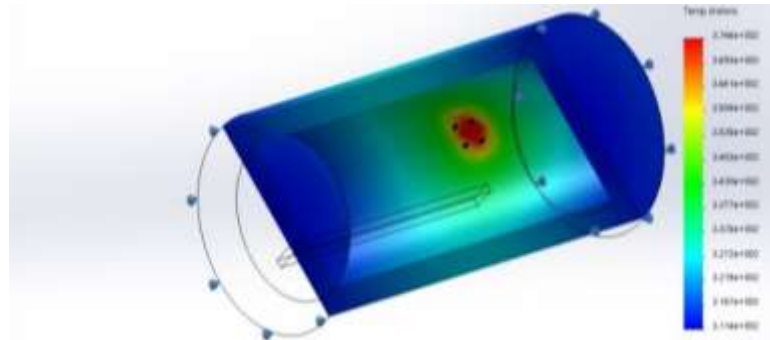

Fig. 5: Faraday cup heat transfer analysis. Heat applied to the middle and convection on each side.

As expected, copper has a lower temperature gradient, since its heat conduction coefficient is about four times larger than that of Molybdenum. Therefore, our worst-case scenario is a material with the heat conduction coefficient of k=100W/mK, which still gives us an acceptable ΔT of 100 degrees. It is important to mention that the convection coefficient was set to h=10 kW/m²K placed at the 2 edges of the Faraday Cup, about 8[mm] away from the center.

3.1. The Cooling Mechanism of the Front Slit
The development process of the cooling method and the smaller details of the exact geometry of the heat exchanger are the focus of the study. Many intricate changes were made in the system until the final product was accepted. The heat exchanger was transformed in many ways from its initial form. Numerous numerical calculations were carried out using different initial conditions and geometries until converging on a solution that was considered satisfactory. We present the geometry in Figure 6**Error! Reference source not found.**. A lot of inspiration for the inclusion of a protective plate to cover the scanner plate has been taken from the work of Rathke [5].
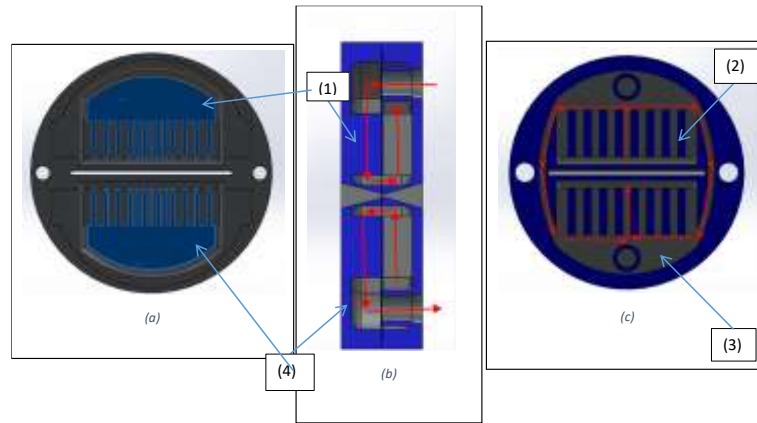
Fig. 6: The geometry of cooling mechanism. (a) Protective plate, (b) Side view of the cooling mechanism, (c) Scanner plate view.

The two front plates (Figure 6a, and 6c), protective and scanner, are mirror images of each other. Using a milling machine, the cavities and the flow channels were created (these double as fins) throughout the solid. The flow, starts at the very top of the mechanism (Figure 6c). Water flows in through the scanner plate and into the first (1) cavity at the top of the protective plate. There the water goes through a series of fins, positioned at 0.5mm spacing from each other, at a width of 0.5mm. Additionally, 6 fins are positioned in the center as opposed to the other 4 on each side (from the centerline) with a width of 1mm and spacing of 1mm. The water is then channeled through a large rectangular passage into the 2nd cavity (2), placed within the scanner plate. The water flows upwards through an array of fins with equal spacing, since the heat load is less significant in this plate. When the water reaches the top of the cavity there are 2 channels, one on each side, where the water can flow to the bottom of the scanner plate, and into the 3rd cavity (3). This 3rd cavity is identical to the 2nd cavity (2) and has the same type of fin array and a rectangular opening where the water can flow into the 4th cavity (4). Cavity number 4 has the same fin set up as cavity (1) and is stationed at the bottom of the protective plate, where the outlet pipe is located.

From a heat transfer point of view, an analytical solution to the problem could not be achieved realistically within the time allowance. Numerical solutions and approximations were exhaustively calculated. The flow mechanics and heat transfer equations solved by the program often incorporate functions where variable density, viscosity, and temperatures along with other variables are taken into account parametrically. A solution is reached through an iterative process and validated only when all parameters converge within an acceptable range. For our purposes 10^{-6} was chosen to be the difference between the value of each parameter on the current iteration and the previous one $x_n-x_{n-1}<10^{-6}$.

3.2. Result summary

The work regarding this mechanism involves a great deal of heat and flow simulations using numerical methods. The conditions the device can realistically withstand are modeled through the numerical simulation. The boundary conditions for continuity, momentum, and energy when performing the numerical calculations is as follows: $dQ/dt=0.1kg/s$, $T_{H2O,in}=293K$, $P_{out}=1$ atm, $T_{D1}=850K$, $T_{D2}=650K$. These boundary conditions are dictated by the equipment at the accelerator facility. The pumps at our disposal can withstand a pressure potential of up to 5 [atm]; this variable will decide the flow rate of the water. The temperature of the cooling water in the reservoir at the facility is set at 20 degrees Celsius. The static temperatures that act on the device are derived from the heat transfer simulation; the worst-case scenario was taken into consideration when performing these simulations - in reality there is much more flexibility for the values of these variables. The requirements of the study demand that the water cooling the device return at a temperature of up to 50 degrees Celsius. With different reservoirs, the returning water temperature can be even higher, where the cooling mechanism can withstand a higher heat load. Different flow rates are also possible for the coolant. With stronger pumps higher flow rates can be achieved, resulting in either lower returning temperature or higher maximum heat load. Figure 7 shows the expected temperatures in the solid under full load: approximately 520°C in the middle area of the front plate; approximately 386°C in the outer ring around the center of the front plate; in the

cross-section view (b) we can see the distribution to the depth of the solid, which is quite similar to the distribution on the front face
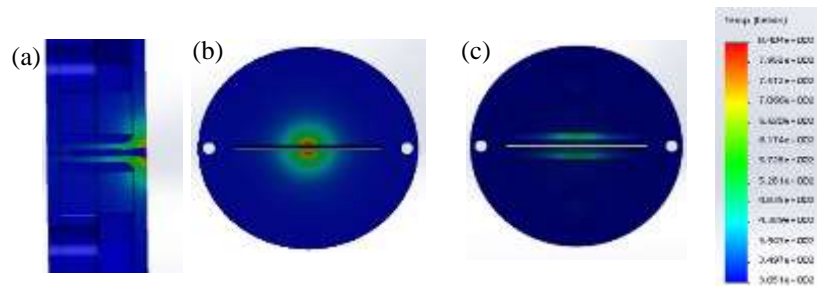

Fig. 7: Heat transfer results of the frontal complex. a) cross section side view of the assembly, b) front view of the protective plate, c) front view, mid-section of the assembly.

Figure 8 (a) and (b) present the isometric and cross-section views, respectively, of the entire scanner complex. There are various attributes to this device with many functions to fit all the required sensory equipment in a compact manner. In Figure 8 (c) the fluid temperature distribution is shown through particle injection from the inlet. What's important to draw here is that the ΔT between inlet and outlet is less than 30°C.
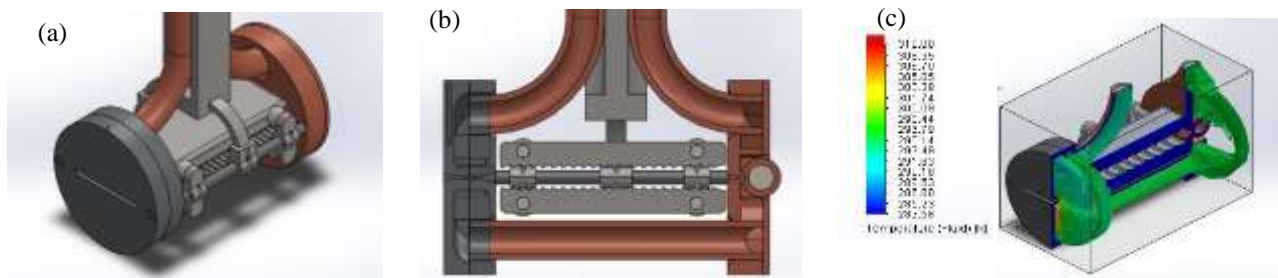

Fig. 8: Final mechanical design assembly of the scanner and the cooling mechanism; isometric (a) and cross-section (b) views; (c) fluid temperature throughout the device.

4. Conclusion

The study produced a state-of-the-art mechanical and thermal design for a miniature Allison emittance scanner. The design consists of a variation of the original Allison emittance scanner. A heat exchanger was fitted into the Allison scanner on a miniature scale allowing the device to perform an emittance measurement on the ion beam within the accelerator beam path. The requirements of the device were fulfilled to their fullest; the numerical calculations showed the device stays within a safe temperature range. The pressure potential remains within adequate range, and the cooling medium returns to the reservoir under 50°C.

Physically, the device successfully fits within the 30×30×50mm³ (width×height×length) dimensions. The thermal and mechanical designs make this design a world-first in Allison emittance scanner class particle accelerator diagnostic tools.

References

[1] A. Feschenko, V. Gaidash, Yu. Kisselev, L. Kravchuk, A. Liyu, A. Menshov, A. Mirzojan, S. Assadi, W. Blokland, S. Henderson, D.-O. Jeon, E. Tanke, "The first results of bunch shape measurements in the SNS linac," *Proceedings of linac,* Lubeck, 2004, pp. 408-410.
[2] P. Forck, "Lecture note on beam instrumentation and diagnostics," *Joint University Accelerator School*, Darmstadt, pp. 1-143, 2003.
[3] M. P. Stockli and R. F. Welton, "Emittance Scanner Optimization for Low-Energy Ion Beams," *Proceedings of the 2005 Particle Accelerator Conference*, 2005, pp. 2705-2707.

[4] P. W. Allison, J. 0. Sherman, and D. Holtkamp, "An emittance scanner for intense low-energy ion beams," *IEEE Transactions on Nuclear Science*, vol. NS-30, no. 4, 1983.

[5] J. Rathke, M. Peacock, and J. J. Sredniawski, "Thermo-Mechanical Design of a CW Sweep Plate Emittance Scanner," 1996.

[6] A. Edelstein, D. Daddoune, I. Silberman, V. Haslavski, "Allison Emittance Scanner project," *Azrieli Jerusalem College of Engineering*, September 2016, Senior design project.

[7] T. A. Thornton and J. N. Anno, "Secondary electron emission from 0.5-2.5 MeV protons and deuterons," *J. Appl. Phys.*, vol. 48, pp. 1718-1719, 1977.

[8] J. E. Borovsky and D. Suszcynsky, "Experimental investigation of the Z2 scaling law of fast-ion-produced secondary-electron emission," *Phys. Rev. A,* vol. 43*,* pp. 1416-1432, 1991.

[9] L. N. Large and W. S. Whitlock, "Secondary electron emission from clean metal surfaces bombarded by fast hydrogen ions," *Proc. Phys. Soc. 79*, pp. 148-157, 1962.

[10] R. A. Baragiola, E. V. Alonso and A. O. Florio, "Electron emission from clean metal surfaces induced by low-energy light ions," *Physical Review B 19.1*, vol. 121, 1979.

[11] E. W. Thomas, ed., "Secondary Electron Emission by Heavy Particle Impact," *Atomic Data for Fusion, Particle Interactions with Surfaces*, vol. 3, ORNL-6088, 1985.

[12] E.W. Thomas, "Particle-Impact Induced Electron Ejection From Surfaces," *International Atomic Energy Agency*, INDC (NDS)-322, pp. 1-52, 1995.

[13] K-H. Schartner. (1998), Particle-Solid Interactions - Ion Induced Electron Emission - Tables of Ion Induced Electron Yields, [Online]. Available: http://www.uni-giessen.de/1.physik/schartner/atom/psi/EEData.html .

[14] J. S. Allen, "The emission of secondary electrons from metals bombarded with protons," *Phys. Rev.,* vol. 55, pp. 336, 1939.

[15] C. Deibele, "Proposal for the Design of the Fast Faraday Cup to Measure the Longitudinal Profile of the 2.5 MeV Beam After the RFQ at the SNS," *SNS internal report no. 0004,* pp. 1-8, 2001.

[16] A. Schultz and M. Pomerantz, *Phys. Rev.,* vol. 130, pp. 2135-2141, 1963.

[17] J. F. Ziegler and J. P. Biersack, "SRIM 2003 - computer program developed by for calculating the stopping and range of ions into matter," 2003.